Photon spheres and shadows of black holes with modified entropy-inspired metrics*

Fang Liu (刘芳)[1,2†] Yu-Bo Ma (马宇波)[1,2‡] Yun-Zhi Du (杜云芝)[1,2§] Huai-Fan Li (李怀繁)[2,3¶]

[1]Department of Physics, Shanxi Datong University, Datong 037009, China
[2]Insitute of Theoretical Physics, Shanxi Datong University, Datong 037009, China
[3]College of General Education, Shanxi College of Technology, Shuozhou 036000, China

Abstract: Starting from the first law of black hole thermodynamics, we establish an explicit correspondence between the corrected entropy and the metric function under the condition of fixed black hole energy and horizon location. Using the corrected metric, we then compute the photon sphere radius and shadow size, demonstrating that different entropy corrections produce characteristic optical shifts. By comparing these results with Event Horizon Telescope observations of Sgr A*, we constrain the parameter range associated with the corrected entropy. This analysis provides a feasible approach for testing generalized entropy frameworks and probing deviations from the Bekenstein--Hawking area law.

Keywords: corrected black hole entropy, photon sphere, black hole shadow

DOI: 10.1088/1674-1137/ae9916 **CSTR:** 32044.14.ChinesePhysicsC.50115110

I. INTRODUCTION

The connections among gravity, thermodynamics, and quantum theory have proven highly useful for studying the structure of spacetime. Since the pioneering work of Bekenstein and Hawking revealed that black holes behave as thermodynamic objects with well-defined temperature and entropy, it has become evident that the laws of gravity are closely linked to thermodynamic structures [1−6].

One of the most profound predictions of general relativity is the deflection of light in curved spacetimes, known as gravitational lensing. Gravitational lensing has emerged as a crucial tool for addressing fundamental problems in astrophysics and cosmology. Research on gravitational lensing in the strong-field regime, particularly near compact objects such as black holes and neutron stars, began in the 1970s [7]. Since then, extensive studies have examined gravitational lensing caused by a wide range of structures, including dark matter, dark energy, quasars, gravitational waves, and other compact objects [8−12].

Near black holes, the most mysterious objects in the universe, light is not merely swallowed; it may also be temporarily trapped. Theoretically, a special spherical surface known as the photon sphere exists just outside the black hole event horizon, where gravity is strong enough to force photons to move along closed orbits, forming a short-lived and highly unstable "photon cage". Any small perturbation causes photons either to fall into the event horizon or to escape to infinity. On April 10, 2019, astronomers worldwide jointly released the first image of a black hole [13−15], and the photon sphere serves as the key structure underlying these images. The optical detection of the supermassive black hole at the Galactic center, Sgr A* (represented by the first black hole shadow image released by the Event Horizon Telescope (EHT)), stands as a landmark triumph for general relativity. Its far-reaching theoretical significance, however, lies in the following: for the first time, the exploration of gravity has transcended the weak-field approximation and entered an entirely new regime encompassing strong gravitational fields, dynamical spacetime, and quantum effects, while also providing a practical instrument for stringently constraining a broad spectrum of new physics theories. In essence, the optical imaging of Sgr A* marks a revolutionary leap in gravitational testing methodologies: from "hearing" gravity via gravitational waves to "seeing" it

Received 18 May 2026; Accepted 12 August 2026; Accepted manuscript online 13 August 2026

* Supported by the National Natural Science Foundation of China (12375050), the Natural Science Foundation of Shanxi Province (202303021211180, 202203021221209, 202203021221211, 202503021211241), the Program for the Innovative Talents of Higher Education Institutions of Shanxi (2024Q030), and the Doctoral Sustentation Fund of Shanxi Datong University

† E-mail: fangliuphys@sxdtdx.edu.cn
‡ E-mail: yuboma.phy@gmail.com
§ E-mail: duyzh13@lzu.edu.cn
¶ E-mail: huaifan.li@stu.xjtu.edu.cn

©2026 Chinese Physical Society and the Institute of High Energy Physics of the Chinese Academy of Sciences and the Institute of Modern Physics of the Chinese Academy of Sciences and IOP Publishing Ltd. All rights, including for text and data mining, AI training, and similar technologies, are reserved.

through electromagnetic radiation. This breakthrough ushers observational and theoretical investigations in strong-gravity astronomy into an unprecedented era of high-precision research. In particular, the black hole shadow observed in these images is closely related to the properties of the photon sphere and the strong gravitational lensing effect near the event horizon. In recent years, the study of photon spheres and black hole shadows has attracted considerable interest, with many works investigating the photon spheres and shadow images of various black hole models. Moreover, photon spheres can provide valuable insights into the physical properties and characteristics of black holes. They can reveal nontrivial features related to spacetime singularities, event horizons, causal structures, and asymptotic behaviors associated with black holes and ultracompact objects. Significant differences exist in the size and morphology of shadows cast by different types of black holes, offering important clues for probing black hole properties and serving as a powerful tool for estimating black hole parameters and testing general relativity, as well as alternative modified theories of gravity [16−58].

Significant progress has also been made in understanding photon spheres and black hole shadows from a geometric perspective. For static, spherically symmetric spacetimes, the photon sphere can be characterized by the vanishing of geodesic curvature and Gaussian optical curvature, providing a coordinate-invariant framework for investigating circular null geodesics. Recently, the authors of [59] systematically studied the gravitational lensing effect and the dynamical evolution of the shadow of the Vaidya black hole using backward ray-tracing techniques, paving the way for exploring the optical properties of nonstationary black holes. The authors of [24] investigated the relation between the number of stable and unstable photon spheres outside the black hole horizon. Motivated by these developments, recent studies on the optical properties of various deformed black holes have attracted our attention [60−66]. The relationships among the location of the black hole photon sphere, critical impact parameters, and the effective potential are among the key issues of widespread concern. Compared with Schwarzschild black holes, black holes with quantum corrections generally possess larger radii for the event horizon, photon sphere, and photon ring, along with a lower effective potential for photons. This conjecture has been widely accepted in the community [67, 68]. By contrast, typical black holes in nonlinear electrodynamics exhibit opposite behavior relative to Schwarzschild black holes: their event horizon, photon sphere, and photon ring radii are smaller, whereas the photon effective potential becomes higher [69, 70]. Our analysis further reveals that distinct conclusions can be drawn for different entropy corrections.

A central goal of modern theoretical physics is to understand the microscopic origin of black hole entropy. Since Bekenstein and Hawking proposed that black hole entropy is proportional to the area of its event horizon, the concept of corrected Bekenstein-Hawking entropy has attracted extensive research attention [71−74]. Corrected Bekenstein-Hawking entropy serves as an important bridge connecting general relativity with quantum gravity theories. From loop quantum gravity to string theory, diverse theoretical frameworks predict correction terms to the entropy, including logarithmic corrections, nonextensive entropies (such as Rényi entropy and Sharma-Mittal entropy), and Barrow entropy, which accounts for quantum gravity fluctuations. Any modification to the Bekenstein-Hawking entropy-area relation induces a corresponding deviation in the spacetime metric, which in turn directly alters the position, stability, and even topological properties of the photon sphere. Recently, the authors of [75, 76] demonstrated that, starting from a chosen corrected entropy functional, one can systematically derive the associated modified metric and its effective matter sector, thereby establishing a direct entropy-geometry correspondence. Furthermore, by comparison with Event Horizon Telescope observations of Sgr A* at the Galactic center, quantitative constraints were imposed on the parameters introduced in the corrected entropy. Very recently, the authors of [77] derived the van der Waals black hole by imposing the condition that the temperature of the van der Waals system equals the Hawking radiation temperature of the black hole. Inspired by this idea, and based on the first law of thermodynamics satisfied by any thermodynamic system, we investigate the effects of different generalized entropies on the spacetime structure of black holes. First, we apply the first law of thermodynamics to obtain the black hole radiation temperature corresponding to various entropy corrections. It should be noted that, under the same spacetime background, the event horizon of the black hole should remain unchanged for different entropy corrections. For the Schwarzschild black hole, $r_+ = 2M$ is held fixed. Under these two constraints, we construct the relation between the corrected entropy and the spacetime metric. We obtain the metric corresponding to the corrected entropy that preserves the fixed horizon position r_+ and $r_+ = 2M$, as well as the black hole radiation temperature $T = \left.\dfrac{f'(r,\alpha,\beta\cdots)}{4\pi}\right|_{r=r_+}$, where T denotes the temperature at which spacetime thermodynamic quantities satisfy the first law of thermodynamics after entropy correction.

The structure of this paper is organized as follows. In Section II, we briefly review various entropy corrections. In Section III, using the metric consistent with the corrected entropy, we investigate the photon sphere location and shadow radius of the modified black hole, analyze the influence of each parameter on the photon sphere and black hole shadow, and compare the theoretical results

with the observational data of Sgr A* at the Galactic center to obtain constraints on the corresponding parameters. Concluding remarks and a detailed discussion of the findings are presented in Section V. We use the units $G_d = \hbar = k_B = c = 1$ throughout this paper.

II. NON-EXTENSIVE ENTROPY

Introduced by Constantino Tsallis, non-extensive entropy extends the conventional Boltzmann-Gibbs entropy. This concept is particularly valuable for systems characterized by nonlinearity and strong sensitivity to initial conditions. Unlike Boltzmann-Gibbs entropy, which assumes linear scaling of entropy with system size, non-extensive entropy can describe systems in which such linearity breaks down. Consequently, it has applications across a broad range of fields, including theoretical physics, cosmology, and statistical mechanics. It is particularly relevant to systems with long-range interactions, fractal structures, or memory effects [56, 78].

A. Barrow entropy

Barrow proposed that quantum gravitational corrections could modify the classical smoothness of the event horizon, leading to horizon geometry with fractal features. This modification suggests that the standard area law governing black hole entropy may not hold exactly. To quantify the degree of geometric irregularity, a parameter Δ is introduced to characterize the extent to which the horizon deviates from a smooth two-dimensional surface. Incorporating this modification, the entropy associated with a black hole can be expressed as [79, 80]:

$$S_B = (S_{\rm BH})^{1+\frac{\Delta}{2}}, \qquad S_{\rm BH} = S_B^{\frac{2}{2+\Delta}}, \tag{1}$$

where the parameter satisfies $0 \le \Delta \le 1$. When $\Delta = 0$, the horizon remains undeformed, and the expression reduces to the standard Bekenstein-Hawking entropy. In contrast, nonzero values of Δ capture the effects of the fractal structure induced by quantum gravity. Conceptually, a nonzero Δ indicates that the microstructure of spacetime at the event horizon departs from classical smoothness, potentially reflecting the underlying quantum gravitational degrees of freedom. Thus, Barrow entropy provides an effective framework for modeling these quantum gravitational corrections without requiring a detailed specification of the microscopic theory.

B. Rényi entropy

Rényi entropy is a form of non-extensive entropy that has been employed in studies of black hole thermodynamics [56, 57, 81]. It provides a generalized entropy measure that extends beyond the additive framework of the Bekenstein-Hawking entropy. A key feature of this framework is the parameter λ, which quantifies the deviation of the entropy from extensivity. This generalized entropy construction is valuable for black hole thermodynamics because the microscopic horizon degrees of freedom can exhibit interactions that are not accounted for within conventional Boltzmann-Gibbs statistics. The Rényi entropy associated with a black hole can be expressed as

$$S_R = \frac{1}{\lambda}\ln(1+\lambda S_{\rm BH}),$$
$$S_{\rm BH} = \frac{e^{\lambda S_R}-1}{\lambda}. \tag{2}$$

The parameter λ in non-extensive entropy plays a pivotal role in defining the entropy function. In this expression, the factor $(1+\lambda S_{\rm BH})$ must be dimensionless. Since the physical dimension of $S_{\rm BH}$ is $[L^2]$, the physical dimension of λ is $[L^{-2}]$. From the perspective of thermodynamics and statistical mechanics, the parameter λ in this entropy should satisfy $0 < \lambda < 1$ [57].

C. Sharma-mittal entropy

Sharma-Mittal entropy constitutes another important class of nonextensive entropy that unifies and generalizes both Rényi and Tsallis entropies. This entropy has found prominent applications in cosmology; for instance, it can account for cosmic accelerated expansion through an effective description of vacuum energy. Although various nonextensive entropies have been widely adopted in black hole research, Sharma-Mittal entropy remains underexplored in the context of black hole thermodynamics. This motivates us to investigate the thermodynamic characteristics of black holes from the perspective of Sharma-Mittal entropy, treating black holes as strongly coupled gravitational systems [82–84].

It can be expressed as follows:

$$S_{\rm SM} = \frac{1}{\alpha}\left((1+\beta S_T)^{\frac{\alpha}{\beta}}-1\right),$$
$$dS_{\rm SM} = (1+\beta S_{\rm BH})^{\frac{\alpha}{\beta}-1}dS_{\rm BH},$$
$$\frac{\partial S_{\rm BH}}{\partial S_{\rm SM}} = (1+\alpha S_{\rm SM})^{1-\frac{\beta}{\alpha}}, \tag{3}$$

In this expression, $S_T = \frac{A}{4}$, where $A = 4\pi r_+^2$ and r_+ is the horizon radius, represents the Tsallis entropy. The parameters α and β are free parameters that must be determined by fitting the results to observational data. We note that the factors $(1+\beta S_T)$ and $(1+\alpha S_{\rm SM})$ are dimensionless; therefore, α and β both have dimensions of $[L^{-2}]$. Notably, when $\alpha \to 0$ and $\alpha \to \beta$, the Sharma-Mittal entropy reduces to the Rényi and Tsallis entropies, respectively [85].

III. MODIFIED SPACETIME GEOMETRY FROM MODIFIED HORIZON ENTROPY

In classical general relativity, the standard procedure is to specify an energy-momentum tensor, solve for the metric components, and then compute the corresponding horizon entropy. Conversely, concepts such as emergent gravity and the holographic principle suggest that gravity may arise from entropic or informational degrees of freedom, emphasizing the fundamental role of entropy. Guided by this perspective, we propose a straightforward approach in which the spacetime geometry is derived directly from the horizon entropy.

The general static spherically symmetric line element is given by

$$\mathrm{d}s = -f(r)\mathrm{d}t^2 + f^{-1}(r)\mathrm{d}r^2 + r^2(\mathrm{d}\theta^2 + \sin^2\theta\mathrm{d}\varphi^2), \tag{4}$$

The event horizon r_+ is defined by $f(r_+) = 0$, and the Hawking temperature is obtained from $T_{\rm BH} = f'(r_+)/4\pi$. The first law of black hole thermodynamics is written as follows:

$$\mathrm{d}M = T_{\rm BH}\mathrm{d}S_{\rm BH}. \tag{5}$$

For a static, spherically symmetric spacetime, when the Bekenstein-Hawking entropy $S_{\rm BH}$ of the black hole is corrected to S, the state parameters of the black hole must satisfy the first law of thermodynamics, namely

$$T = \frac{\kappa}{2\pi} = \frac{f'(r_+)}{4\pi} = \frac{\partial M}{\partial S} = \frac{\partial M}{\partial S_{\rm BH}}\frac{\partial S_{\rm BH}}{\partial S} = T_{\rm BH}\frac{\partial S_{\rm BH}}{\partial S}. \tag{6}$$

Note that the parameters introduced through entropy corrections are treated as constants. How corrected entropy affects the spacetime geometry of black holes is a question of broad interest. Recently, the authors of [75, 76] proposed an entropy-geometry correspondence scheme to address modifications of the spacetime metric induced by corrected entropy. A key aspect of this approach is to replace the coordinate function r in the Schwarzschild metric with S, thereby determining the influence of entropy corrections on the metric and the resulting photon sphere. The authors of [77] proposed imposing the condition that the temperature of the van der Waals system equals the Hawking temperature of the black hole, yielding the spacetime metric corresponding to the van der Waals black hole. This idea has opened a new avenue for investigating metric modifications induced by corrected entropy. The correction of black hole entropy arises from attempts to incorporate the effects of quantum gravity theories into classical black hole thermodynamics. Regardless of the method used to obtain the entropy correction terms, the main constraints are to keep the black hole's parameter M constant, leave the position of the black hole's event horizon unchanged, and ensure that the black hole's thermodynamic quantities satisfy the first law of thermodynamics. We now discuss how to derive the spacetime metric corresponding to entropy corrections under these constraints.

We assume that the backreaction induced by an arbitrary entropy function can be reflected in the spacetime metric; that is, the Schwarzschild metric Eq. (4) is modified to

$$\begin{aligned}\mathrm{d}s = &-f(r,\alpha,\beta\cdots)\mathrm{d}t^2 + f^{-1}(r,\alpha,\beta\cdots)\mathrm{d}r^2 \\ &+ r^2(\mathrm{d}\theta^2 + \sin^2\theta\mathrm{d}\varphi^2),\end{aligned} \tag{7}$$

where $\alpha,\beta,\cdots$ denote the parameters introduced by different entropy corrections. These parameters are required to satisfy

$$\frac{1}{4\pi}\frac{\partial f(r,\alpha,\beta,\cdots)}{\partial r}\bigg|_{r=r_+} = T, \tag{8}$$

where T is given by Eq. (6). Second, the position of the black hole event horizon r_+ must satisfy $f(r_+,\alpha,\beta,\cdots) = 0$, under the condition that $r_+ = 2M$ remains unchanged. Under these constraints, we take

$$f(r,\alpha,\beta,\cdots) = \frac{\partial S_{\rm BH}}{\partial S}f(r), \tag{9}$$

where $f(r) = 1 - \dfrac{2M}{r}$. Since the photon sphere is located outside the horizon, typically at $r \sim 3M$ in the Schwarzschild case, its position and the shadow radius are sensitive to the extension of the metric away from the horizon. One can add corrections satisfying

$$\delta f(r_+) = 0, \qquad \delta f'(r_+) = 0. \tag{10}$$

Hence, Eq. (9) indicates that the corrected black hole event horizon depends on $\dfrac{\partial S_{\rm BH}}{\partial S} = 0$ or $f(r)$. From Eqs. (1), (2), and (3), we find that $\dfrac{\partial S_{\rm BH}}{\partial S} \neq 0$, which preserves the same horizon position but changes the radius of the photon sphere. Furthermore, Eq. (9) must reduce to the Schwarzschild black hole case when all parameters $\alpha,\beta,\cdots$ are set to zero. To investigate the influence of entropy on the metric, we adopt the method proposed in Refs. [75, 76] for extending the black hole horizon relation; that is, we extend the Bekenstein-Hawking entropy $S_{\rm BH} = \pi r_+^2$ to $S_{\rm BH} \to \pi r^2$ and replace r_+ in the various corrected entropies with r.

Thus, the components of the Einstein tensor G^{μ}_{ν} can be calculated from the metric (9). As shown in Ref. [86]

$$G_t^t = G_r^r = \frac{1}{r}\frac{\mathrm{d}f(r,\alpha,\beta,\cdots)}{\mathrm{d}r} + \frac{f(r,\alpha,\beta,\cdots)-1}{r^2}, \tag{11}$$

$$G_\theta^\theta = \frac{\mathrm{d}^2 f(r,\alpha,\beta,\cdots)}{2\mathrm{d}r^2} + \frac{1}{r}\frac{\mathrm{d}f(r,\alpha,\beta,\cdots)}{\mathrm{d}r}. \tag{12}$$

From the field equations of general relativity

$$G_\nu^\mu = 8\pi T_\nu^\mu, \tag{13}$$

We conclude that a nonzero effective stress-energy tensor arising from the Extended Generalized Uncertainty Principle (EGUP) can be obtained. In particular, we define $T_\nu^\mu = (-\rho, p_r, p_t, p_t)$, where

$$\rho = -G_t^t, \quad \rho = -p_r, \quad p_t = G_\theta^\theta. \tag{14}$$

It should be noted that this relation reflects a radial equation of state similar to that of vacuum or dark energy [61, 75, 76]. However, because $p_r \neq p_t$, the effective matter sector arising from entropy is anisotropic. Consequently, the deviation of the entropy function from the standard area law acts as a geometric source, generating an anisotropic stress-energy tensor without requiring the introduction of explicit matter fields. In this sense, the corrected entropy manifests as an effective, emergent gravitational matter content associated with the microscopic structure of the horizon. This conclusion is consistent with the discussions in Refs. [75, 76] and with results obtained by considering the generalized uncertainty principle [66].

The motion of massless photons along geodesics is governed by the Lagrangian density [43, 44, 87, 88]

$$H = \frac{1}{2} g^{\mu\nu} p_\mu p_\nu = 0, \tag{15}$$

where $p_\mu = \dfrac{\mathrm{d}x_\mu}{\mathrm{d}\lambda}$ denotes the generalized momentum, and λ is the affine parameter. Owing to the spherical symmetry of this system, we focus on equatorial geodesics with $\theta = \pi/2$, for which the Lagrangian simplifies to

$$-f(r,\alpha,\beta,\cdots)\left(\frac{\mathrm{d}t}{\mathrm{d}\tau}\right)^2 + f^{-1}f(r,\alpha,\beta,\cdots)\left(\frac{\mathrm{d}r}{\mathrm{d}\tau}\right)^2 + r^2\left(\frac{\mathrm{d}\varphi}{\mathrm{d}\tau}\right)^2 = 0, \tag{16}$$

where τ denotes the proper time. Moreover, the static, spherically symmetric spacetime admits two conserved quantities, given by

$$E = -\frac{\partial H}{\partial \dot{t}} = f(r,\alpha,\beta,\cdots)\dot{t}, \quad \bar{L} = -\frac{\partial H}{\partial \dot{\varphi}} = r^2\dot{\varphi}. \tag{17}$$

Using $\mathrm{d}s^2 = 0$, the radial component of the geodesic equations can be expressed as

$$\frac{1}{b^2} = \left(\frac{\mathrm{d}r}{\mathrm{d}\lambda}\right)^2 + \frac{f(r,\alpha,\beta,\cdots)}{r^2}. \tag{18}$$

We rescale the affine parameter λ by $\lambda/|L|$, where $b = |L|/E$ denotes the impact parameter, and L and E are the conserved angular momentum and energy of the photons, respectively. From Eq. (16), the effective potential governing the propagation of light rays is defined as

$$V_{\mathrm{eff}}(r) = \frac{\sqrt{f(r,\alpha,\beta,\cdots)}}{r}. \tag{19}$$

The radius r_{ph} of unstable circular null geodesics, which form a photon sphere, is determined by the following conditions

$$V_{\mathrm{eff}}(r_{\mathrm{ph}}) = \frac{1}{b_{\mathrm{ph}}}, \quad V'_{\mathrm{eff}}(r_{\mathrm{ph}}) = 0, \quad V''_{\mathrm{eff}}(r_{\mathrm{ph}}) < 0, \tag{20}$$

where b_{ph} is the corresponding impact parameter.

For a fixed impact parameter, the radial motion of photons can be treated analogously to that of a particle in a classical potential field, such as a gravitational or centrifugal potential. This analogy facilitates visualization of the photon's dynamical evolution. Here, the radius of the unstable photon sphere is denoted by $r_p h$, which is determined by the implicit expression

$$r_{\mathrm{ph}} f'(r_{\mathrm{ph}},\alpha,\beta,\cdots) - 2f(r_{\mathrm{ph}},\alpha,\beta,\cdots) = 0. \tag{21}$$

The critical impact parameter is given by

$$b_{\mathrm{ps}} = \frac{\bar{L}}{E_c} = \left.\frac{r}{\sqrt{f(r,\alpha,\beta,\cdots)}}\right|_{r_{\mathrm{ph}}}. \tag{22}$$

IV. APPLICATION OF DIFFERENT ENTROPY CORRECTIONS

A. Barrow entropy

Substituting Eq. (1) into Eq. (9), we obtain the spacetime metric corresponding to Barrow entropy.

$$f_B(r,\Delta) = \frac{2}{(2+\Delta)\pi^{\Delta/2} r^\Delta} f(r). \tag{23}$$

From Eq. (23), the position of the black hole's event horizon is determined by $f(r_+) = 0$, the black hole's radiation temperature is $T = \dfrac{1}{4\pi}\left(\dfrac{\partial S_{\mathrm{BH}}}{\partial S}\right)_{r=r_+} f'(r_+)$, and the

black hole parameter is M. As shown in Eq. (23), when $0<\Delta<1$ and $r>2M$, the factor $\frac{2}{(2+\Delta)\pi^{\Delta/2}r^{\Delta}}$ is smooth, indicating that $f_B(r,\Delta)$ has no horizons other than the event horizon at $r=2M$. The Kretschmann scalar

$$R_{\mu\nu\rho\sigma}R^{\mu\nu\rho\sigma} = \frac{4-8f_B(r,\Delta)+4f_B^2(r,\Delta)+4r^2f_B'^2(r,\Delta)+r^4f_B''^2(r,\Delta)}{r^4}. \quad (24)$$

Outside the event horizon, the curvature quantities remain finite and regular everywhere.

From Eqs. (11) and (12), we obtain

$$\begin{aligned} G_t^t =& G_r^r = \frac{2}{(2+\Delta)\pi^{\Delta/2}r^{\Delta+2}}\left(\frac{2M\Delta}{r}-\Delta+1\right)-\frac{1}{r^2},\\ G_t^t =& G_r^r = \frac{2\Delta}{(2+\Delta)\pi^{\Delta/2}r^{\Delta+2}}\left(\frac{2M-r}{r}\right)\\ &+\frac{1}{r^{2+\Delta}}\left(\frac{2}{(2+\Delta)\pi^{\Delta/2}}-r^{\Delta}\right),\\ G_{\varphi}^{\varphi} =& G_{\theta}^{\theta} = \frac{2}{(2+\Delta)\pi^{\Delta/2}r^{\Delta+2}}\left(\frac{2M\Delta}{r}-\Delta+1\right)-\frac{1}{r^2}. \end{aligned} \quad (25)$$

For $0\le\Delta\le1$, because $r\ge2M$, $\frac{2\Delta}{(2+\Delta)\pi^{\Delta/2}r^{\Delta+2}}\left(\frac{2M-r}{r}\right)\le0$. Taking $M=1$ gives $r\ge2$; hence, $\left(\frac{2}{(2+\Delta)\pi^{\Delta/2}}-r^{\Delta}\right)\le0$. When $\Delta=0$, the metric reduces to the Schwarzschild vacuum.

We now briefly examine the energy conditions of the corrected spacetime. For $M>0$ and $\Delta>0$, the effective energy density is positive, $\rho>0$. Since $\rho+p_r=0$ holds along the radial null direction, the null energy condition (NEC) is saturated. Along the tangential direction, we obtain $\rho+p_t=0$, which also saturates the NEC. Furthermore, $\rho>0$ ensures that the weak energy condition (WEC) is satisfied. We find that $\rho+p_r+2p_t=2p\le0$, implying that the strong energy condition (SEC) is violated. The dominant energy condition (DEC) holds only when $\rho>0$ and $|p_i|\le\rho$. As observed, the effective matter sector behaves as an isotropic fluid with positive energy density and an isotropic pressure satisfying $p=-\rho$. Such stress-energy configurations cannot be produced by conventional classical matter and arise from the quantum-gravitational or fractal corrections introduced by the Barrow entropy modification. Therefore, the SEC violation is not a pathological feature of the spacetime; rather, it indicates the existence of an effective non-classical matter source that sustains the modified horizon geometry [75]. Substituting Eq. (23) into Eq. (19), we obtain

$$V_{\rm eff}(r)=\frac{1}{r}\sqrt{\frac{2}{(2+\Delta)\pi^{\Delta/2}r^{\Delta}}f(r)}. \quad (26)$$

Setting $r=M\eta$ $(2<\eta<\infty)$, we obtain

$$(M)^{1+\Delta/4}V_{\rm eff}(\eta)=\frac{1}{\eta^{1+\Delta/4}}\sqrt{\frac{2}{(2+\Delta)\pi^{\Delta/2}}\left(1-\frac{2}{\eta}\right)}. \quad (27)$$

For different values of Δ, we obtain the corresponding $(2M)^{1+\Delta/4}V_{\rm eff}(\eta)-\eta$ curves based on Eq. (27), as shown in Fig. 1.

Substituting Eq. (23) into Eqs. (21) and (22), we obtain

$$\begin{aligned} r_{\rm ph\Delta} &= \frac{2M(3+\Delta)}{2+\Delta},\\ b_{\rm ps\Delta} &= \frac{\sqrt{2}M(3+\Delta)^{3/2}\pi^{\Delta/4}}{(2+\Delta)^{1/2}}\left(\frac{2M(3+\Delta)}{2+\Delta}\right)^{\Delta/2}. \end{aligned} \quad (28)$$

Here, $r_{\rm ph\Delta}$ and $b_{\rm ps\Delta}$ denote the photon sphere radius and the corresponding critical impact parameter of the black hole with Barrow entropy.

Figure 2 presents the $r_{\rm ph\Delta}-\Delta$ and $b_{\rm ps\Delta}-\Delta$ curves for $M=1$ and $0\le\Delta\le1$. Figures 1 and 2 show that, as the entropy correction parameter Δ increases, the maximum value of the effective potential decreases, the photon-sphere radius $r_{\rm ph\Delta}$ decreases, whereas the critical impact parameter $b_{\rm ph\Delta}$ increases.

The latest Very Long Baseline Interferometry (VLBI) observational results for Sagittarius A* from the Event Horizon Telescope (EHT) [89–92] are given by

$$\begin{aligned} &4.55\le b_{\rm ps\alpha}\le5.22,\quad 1.516\le\frac{b_{\rm ps\alpha}}{3}\le1.74,\quad (1\sigma),\\ &4.21\le b_{\rm ps\alpha}\le5.56,\quad 1.403\le\frac{b_{\rm ps\alpha}}{3}\le1.85,\quad (2\sigma). \end{aligned} \quad (29)$$

Constrained by Eq. (29), the Barrow entropy parameter Δ is determined to lie in the range $0\le\Delta\le0.004$ at the

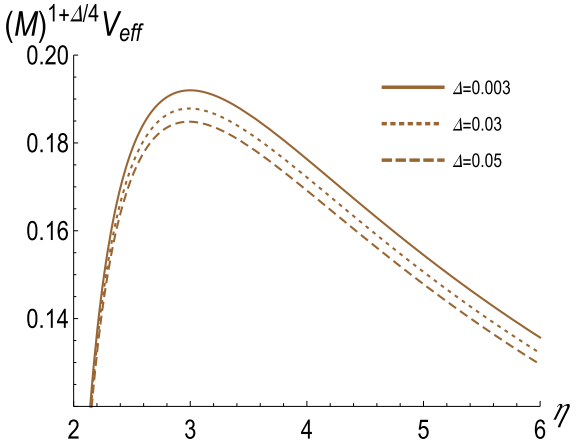


Fig. 1. (color online) The $M^{1+\Delta/4}V_{\rm eff}(\eta)-\eta$ curves for different values of Δ.

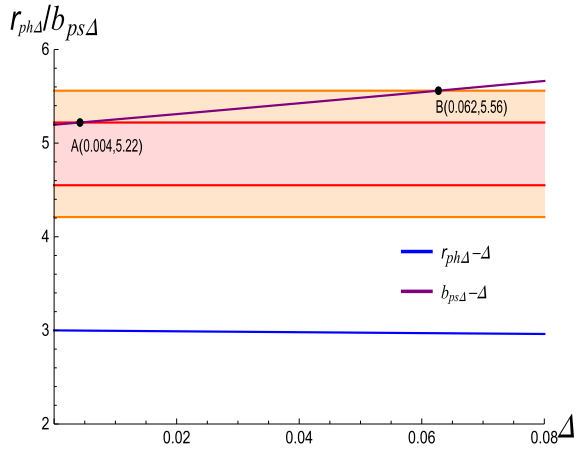


Fig. 2. (color online) The $r_{\rm ph\Delta}-\Delta$ and $b_{\rm ps\Delta}-\Delta$ curves for $M=1$ and $0\le\Delta\le 1$.

1σ level (corresponding to point A in Fig. 2) and $0\le\Delta\le 0.062$ at the 2σ level (corresponding to point B in Fig. 2). The region between the two red lines represents the 1σ constraint interval, whereas the region between the two orange lines represents the 2σ constraint interval.

B. Rényi entropy

Substituting Eq. (2) into Eq. (9) yields the spacetime metric corresponding to the Rényi entropy.

$$f_R(r,\lambda)=(1+\pi\lambda r^2)f(r). \tag{30}$$

As shown in Eq. (30), for $0<\lambda<1$ and $r>2M$, the factor $(1+\pi\lambda r^2)$ is continuous and smooth, indicating that $f_R(r,\lambda)$ admits no horizons other than the event horizon at $r=2M$. In this case, the Kretschmann scalar has the same form as in Eq. (24), and the analysis indicates that it is well behaved and nondivergent.

Using Eqs. (11) and (12), we derive

$$\begin{aligned} G_t^t &= G_r^r = 3\pi\lambda-4\pi\lambda\frac{M}{r}=\pi\lambda\left(3-\frac{4M}{r}\right),\\ G_\theta^\theta &= \pi\lambda\left(3-\frac{2M}{r}\right). \end{aligned} \tag{31}$$

When $\lambda=0$, the metric reduces to the Schwarzschild vacuum. Note that for $M>0$ and $r>2M$, the effective energy density is $\rho<0$. Because $\rho+p_r=0$ along the radial null direction, the NEC is saturated. In the tangential direction, $\rho+p_t=\dfrac{2M}{r}>0$; thus, the NEC is satisfied. Since $\rho<0$, the WEC is violated. We find that $\rho+p_r+2p_t=2p\ge 0$; therefore, the SEC holds. Finally, because the conditions $\rho\ge 0$ and $|p_i|\le\rho$ are not satisfied, the DEC is also violated.

Substituting Eq. (30) into Eq. (19), we obtain

$$V_{\rm eff}(r)=\frac{1}{r}\sqrt{(1+\pi\lambda r^2)f(r)}. \tag{32}$$

Setting $r=3M\eta$ with $\dfrac{2}{3}<\eta<\infty$, we have

$$MV_{\rm eff}(\eta)=\frac{\sqrt{(1+3\chi\frac{\eta^2}{4})\left(1-\frac{2}{3\eta}\right)}}{3\eta}, \tag{33}$$

where $\chi=12\pi\lambda M^2$. For different values of χ, we obtain the corresponding $MV_{\rm eff}-\eta$ curves based on Eq. (33), as shown in Fig. 3.

Substituting Eq. (30) into Eqs. (21) and (22) yields

$$\begin{aligned} \frac{r_{{\rm ph}\lambda}}{3M} &= 2\frac{1-\sqrt{1-\chi}}{\chi},\\ \frac{b_{{\rm ps}\lambda}}{3M} &= \frac{2(1-\sqrt{1-\chi})}{\chi\sqrt{\left(1-\frac{\chi}{3(1-\sqrt{1-\chi})}\right)\left(1+\frac{3}{\chi}\left((1-\sqrt{1-\chi})\right)^2\right)}}. \end{aligned} \tag{34}$$

Here, $r_{{\rm ph}\lambda}$ and $b_{{\rm ps}\lambda}$ denote the photon sphere radius and the corresponding critical impact parameter of the black hole with Rényi entropy. Figure 4 presents the $\dfrac{r_{{\rm ph}\lambda}}{3M}-\chi$ and $\dfrac{b_{{\rm ps}\lambda}}{3M}-\chi$ curves for $M=1$. It can be seen from Fig. 3 and Fig. 4 that, as the entropy correction parameter χ increases, the maximum value of the potential $V_{\rm eff}(\eta)$ and the position of the photon sphere $\dfrac{r_{{\rm ph}\lambda}}{3M}$ increase, whereas the critical impact parameter $\dfrac{b_{{\rm ps}\lambda}}{3M}$ decreases. Subject to Eq. (29), the allowed range of the parameter $\chi(\lambda)$ in the Rényi entropy is determined to be $0\le\chi(\lambda)\le 0.37$, (1σ) (corresponding to point A in Fig. 4) and $0\le\chi(\lambda)\le 0.597$, (2σ) (corresponding to point B in Fig. 4).

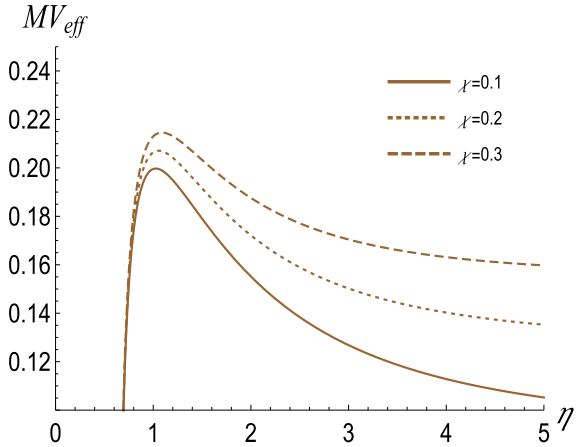


Fig. 3. (color online) The $MV_{\rm eff}$–η curves for different values of χ.

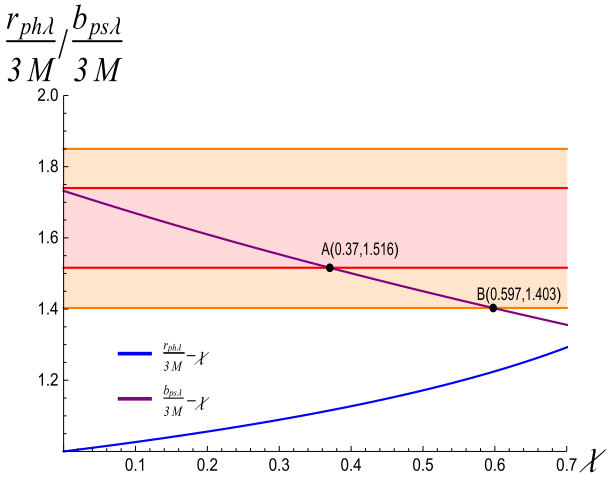


Fig. 4. (color online) The $\frac{r_{\mathrm{ph}\lambda}}{3M}-\chi$ curve and the $\frac{b_{\mathrm{ps}\lambda}}{3M}-\chi$ curve for $M=1$.

Comparing Fig. 2 with Fig. 4 shows that the trends of the photon sphere position r_{ph} and the critical impact parameter b_{ps} with the parameter Δ in the Barrow entropy differ from those with the parameter λ in the Rényi entropy; indeed, the two trends are exactly opposite. From Fig. 1 and Fig. 3, the trends of the effective potential V_{eff} with Δ and λ are also exactly opposite. This indicates that the parameter Δ in the Barrow entropy and the parameter λ in the Rényi entropy play different roles in black hole deformation. The spacetime in Eq. (30) is not asymptotically flat. In such spacetimes, although the critical impact parameter b_{ps} given in Eq. (22) can be defined globally, its direct correspondence to the black hole's shadow size observed by an observer is no longer straightforward. A more precise discussion would require the application of the ray-tracing method. However, for simplicity, this work discusses only the critical impact parameter b_{ps}, and a more quantitative ray-tracing analysis is not considered.

C. Sharma-mittal entropy

Substituting Eq. (3) into Eq. (9) yields the spacetime metric corresponding to the Sharma–Mittal entropy.

$$f_{\mathrm{SM}}(r,\alpha,\beta)=\frac{1}{(1+\pi\beta r^2)^{\frac{\alpha}{\beta}-1}}f(r). \tag{35}$$

As shown in Eq. (35), for $\alpha>0$ and $\beta>0$, the factor $\frac{1}{(1+\pi\beta r^2)^{\frac{\alpha}{\beta}-1}}$ is continuous and smooth for $r>2M$. This indicates that $f_{\mathrm{SM}}(r,\alpha,\beta)$ has no horizons other than the event horizon at $r=2M$. In this case, the Kretschmann scalar has the same form as in Eq. (24), and the analysis indicates that it is well behaved and does not diverge. Using Eqs. (11) and (12), we derive

$$\begin{aligned}G_t^t=G_r^r&=\frac{1}{(1+\pi\beta r^2)^{\frac{\alpha}{\beta}}}\left(2\pi(\beta-\alpha)f(r)+\frac{(1+\pi\beta r^2)}{r^2}\right)-\frac{1}{r^2},\\ G_\varphi^\varphi=G_\theta^\theta&=\frac{\pi(\beta-\alpha)}{(1+\pi\beta r^2)^{\frac{\alpha}{\beta}+1}}[-2\pi\alpha r^2 f(r)\\ &\quad+(1+\pi\beta r^2)f(r)+2(1+\pi\beta r^2)].\end{aligned} \tag{36}$$

As $\alpha\to\beta$, $G_t^t=G_r^r\to 0$ and $G_\theta^\theta\to 0$, so the metric reduces to the Schwarzschild vacuum. For $\alpha\to 0$ with $\beta\geq 0$, we have

$$\begin{aligned}G_t^t=G_r^r&=2\pi\beta f(r)+\pi\beta=\pi\beta\left(3-\frac{4M}{r}\right)\geq 0,\quad \rho\leq 0\\ G_\varphi^\varphi=G_\theta^\theta&=\pi\beta\left[f(r)+2\right]\geq 0.\end{aligned} \tag{37}$$

Note that for $M>0$, $\alpha\geq 0$, $\beta>0$, and $r>2M$, the effective energy density is negative, $\rho<0$. Since $\rho+p_r=0$ along the radial null direction, the NEC is saturated in this direction. In the tangential direction, $\rho+p_t=\frac{4M}{r}>0$; therefore, the NEC holds. Since $\rho<0$, the WEC is violated. We obtain $\rho+p_r+2p_t=\pi\beta\left[f(r)+2\right]\geq 0$, which implies that the SEC is satisfied. Finally, the conditions $\rho\geq 0$ and $|p_i|\leq\rho$ cannot be simultaneously satisfied; therefore, the DEC is also violated. For $\beta>\alpha>0$,

$$\begin{aligned}&G_t^t=G_r^r=\frac{2\pi(\beta-\alpha)}{(1+\pi\beta r^2)^{\frac{\alpha}{\beta}}}f(r)+\frac{(1+\pi\beta r^2)^{1-\frac{\alpha}{\beta}}}{r^2}-\frac{1}{r^2}>0,\quad \rho\leq 0,\\ &G_\varphi^\varphi=G_\theta^\theta>0.\end{aligned} \tag{38}$$

Accordingly, for $\beta>\alpha$, the set of satisfied energy conditions is identical to that in the limit $\alpha\to 0$ with $\beta\geq 0$. The SEC remains satisfied, whereas the DEC is violated because the constraints $\rho\geq 0$ and $|p_i|\leq\rho$ are not satisfied.

Substituting Eq. (35) into Eqs. (21) and (22), we find that the position of the photon sphere satisfies

$$3M+M\pi r_{\mathrm{ph}}^2(2\alpha+\beta)-r_{\mathrm{ph}}-\alpha\pi r_{\mathrm{ph}}^3=0, \tag{39}$$

By introducing the dimensionless parameters $x=\alpha\pi M^2$ and $y=\beta\pi M^2$, and parameterizing $r_{\mathrm{ph}xy}=r_{\mathrm{ph}}=3M\eta$ ($\frac{2}{3}<\eta<\infty$), Eq. (39) can be transformed into

$$1+3\eta^2(2x+y)-\eta-9x\eta^3=0, \tag{40}$$

When $x(\alpha)=0$ and $y(\beta)=0$, Eq. (40) reduces to the

photon sphere position of the Schwarzschild black hole.

In the following, we solve Eq. (40) by considering two cases.

1) When $x(\alpha)=0$.

Eq. (40) can be written as

$$1+3y\eta^2-\eta=0. \tag{41}$$

Solving this equation, we obtain $\eta=\dfrac{1\pm\sqrt{1-12y}}{6y}$. It follows that $0\le y\le\dfrac{1}{12}$, and only the negative sign is admissible. This is because, when the positive sign is chosen and $y\to 0$, η diverges, which does not satisfy the requirement. Thus, we obtain

$$\eta=\frac{1-\sqrt{1-12y}}{6y},\qquad \frac{r_{\rm phy}}{3M}=\frac{1-\sqrt{1-12y}}{6y},$$
$$\frac{b_{\rm psy}}{3M}=\frac{\bar{L}}{E_c}=\left.\frac{r}{\sqrt{f(r,y)}}\right|_{r_{\rm phy}}=$$
$$\frac{1-\sqrt{1-12y}}{6y\sqrt{\left(1+\dfrac{1}{4y}(1-\sqrt{1-12y})^2\right)\left(1-\dfrac{4y}{1-\sqrt{1-12y}}\right)}}. \tag{42}$$

Note that, in this case, $r_{\rm phy}=r_{\rm ph}$ and $b_{\rm psy}=b_{\rm ps}$ denote the photon sphere radius and the corresponding critical impact parameter, respectively, of the black hole with Sharma–Mittal entropy when $x(\alpha)=0$. Figure 5 shows the $\dfrac{r_{\rm phy}}{3M}-y(\beta)$ and $\dfrac{b_{\rm psy}}{3M}-y(\beta)$ curves when $M=1$ and $x(\alpha)=0$. Figs. 6 and 5 show that, when $x(\alpha)=0$, the maximum value of the effective potential $V_{\rm eff}$ increases as $y(\beta)$ increases. For the black hole associated with the Sharma-Mittal entropy, the position of the photon sphere

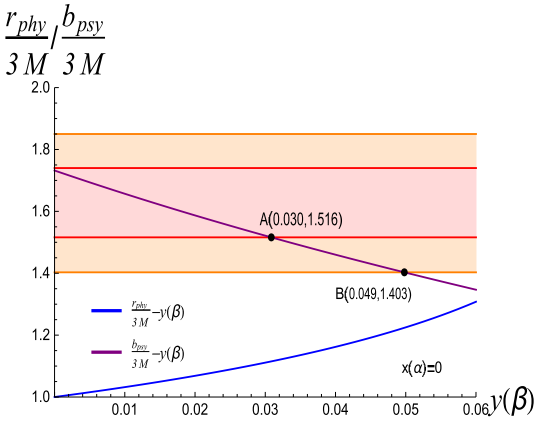


Fig. 5. (color online) The $\dfrac{r_{\rm phy}}{3M}-y(\beta)$ and $\dfrac{b_{\rm psy}}{3M}-y(\beta)$ curves for $M=1$.

$r_{\rm phy}$ increases as $y(\beta)$ increases, whereas the critical impact parameter $b_{\rm psy}$ decreases. Under the constraint in Eq. (29), when $x(\alpha)=0$, the admissible range of the parameter $y(\beta)$ in the Sharma-Mittal entropy is $0\le y(\beta)\le 0.030$ at (1σ) (corresponding to point A in Fig. 5) and $0\le y(\beta)\le 0.049$ at (2σ) (corresponding to point B in Fig. 5).

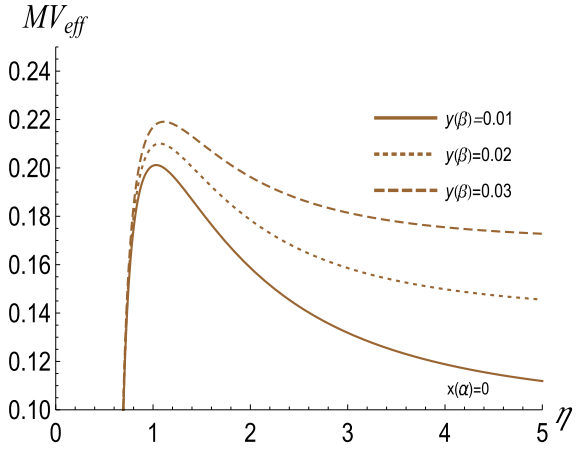


Fig. 6. (color online) The $MV_{\rm eff}-\eta$ curves for different values of $y(\beta)$.

Substituting Eq. (35) into Eq. (19), we obtain

$$MV_{\rm eff}(\eta)=\frac{1}{3\eta}\sqrt{\frac{1}{(1+9y\eta^2)^{\frac{x}{y}-1}}\left(1-\frac{2}{3\eta}\right)}, \tag{43}$$

when $x(\alpha)=0$,

$$MV_{\rm eff}(\eta)=\frac{1}{3\eta}\sqrt{(1+9y\eta^2)\left(1-\frac{2}{3\eta}\right)}. \tag{44}$$

By assigning different values to $y(\beta)$, we obtain the corresponding $MV_{\rm eff}-\eta$ curves based on Eq. (44).

A comparison of Fig. 4 with Fig. 5 shows that the photon sphere position $r_{{\rm ph}\lambda}$ of the black hole associated with the Rényi entropy varies with the correction parameter $y(\beta)$ in a manner similar to the photon sphere position $r_{\rm phy}$ and critical impact parameter $b_{\rm psy}$ of the black hole associated with the Sharma-Mittal entropy when $x(\alpha)=0$. Similarly, a comparison of Fig. 6 with Fig. 3 indicates that the variation patterns of the entropy-corrected effective potential $V_{\rm eff}$ with respect to $r(\eta)$ are also similar. Thus, the optical properties of the black hole associated with the Rényi entropy are similar to those of the black hole associated with the Sharma-Mittal entropy when $x(\alpha)=0$.

2) When $y(\beta)=constant\neq 0$ **or** $x(\alpha)=constant\neq 0$.

The solution to Eq. (40) is

$$\eta = Y + \frac{3(2x+y)}{27x} = Y + \frac{(2x+y)}{9x}, \tag{45}$$

where

$$\begin{aligned} Y &= \sqrt[3]{-\frac{q}{2} + \sqrt{\left(\frac{q}{2}\right)^2 + \left(\frac{p}{3}\right)^3}} + \sqrt[3]{-\frac{q}{2} - \sqrt{\left(\frac{q}{2}\right)^2 + \left(\frac{p}{3}\right)^3}}, \\ p &= -\frac{1}{9x}\left(\frac{(2x+y)^2}{3x} - 1\right), \\ q &= -\frac{1}{9x}\left(1 + 2\frac{(2x+y)^3}{(9x)^2} - \frac{(2x+y)}{9x}\right). \end{aligned} \tag{46}$$

Substitution of Eqs. (45) and (46) into Eqs. (19), (21) and (22) yields

$$MV_{\rm eff}(r,x,y) = \frac{1}{3\eta}\sqrt{(1+9y\eta^2)^{1-\frac{x}{y}}\left(1-\frac{2}{3\eta}\right)}, \tag{47}$$

$$\begin{aligned} \frac{r_{{\rm ph}xy}}{3M} = \eta, \quad \frac{b_{{\rm ps}xy}}{3M} &= \frac{\bar{L}}{E_c} = \left.\frac{r}{\sqrt{f(r,x,y)}}\right|_{r_{{\rm ph}xy}} \\ &= \frac{\eta}{\sqrt{(1+9y\eta^2)^{1-\frac{x}{y}}\left(1-\frac{2}{3\eta}\right)}}. \end{aligned} \tag{48}$$

Here, $r_{{\rm ph}xy} = r_{\rm ph}$ and $b_{{\rm ps}xy} = b_{\rm ps}$ denote the photon sphere radius and the corresponding impact parameter, respectively. In the following, $r_{{\rm ph}xy} = r_{\rm ph} = r_{{\rm ph}x}$ and $b_{{\rm ps}xy} = b_{\rm ps} = b_{{\rm ps}x}$ for a fixed $y(\beta)$, whereas $r_{{\rm ph}xy} = r_{\rm ph} = r_{\rm phy}$ and $b_{{\rm ps}xy} = b_{\rm ps} = b_{\rm psy}$ for a fixed $x(\alpha)$. From Eqs. (45) and (48), for a given $y(\beta)$, we can plot the $\frac{b_{{\rm ps}x}}{3M}-x(\alpha)$ and $\frac{r_{{\rm ph}x}}{3M}-x(\alpha)$ curves. Similarly, for a given $x(\alpha)$, we can plot the $\frac{b_{\rm psy}}{3M}-y(\beta)$ and $\frac{r_{\rm phy}}{3M}-y(\beta)$ curves. Given the constraint conditions satisfied by $x(\alpha)$ and $y(\beta)$, we have also plotted the $MV_{\rm eff}(r,x,y)-\eta$ curves for fixed $x(\alpha)$ or $y(\beta)$ based on Eq. (47).

Figures 7 and 8 show that, for a fixed value of $x(\alpha)$, the photon sphere radius $r_{\rm phy}$ of the black hole associated with Sharma-Mittal entropy increases as the correction parameter $y(\beta)$ rises, whereas the critical impact parameter $b_{\rm psy}$ decreases accordingly. Meanwhile, the maximum value of the effective potential $V_{\rm eff}$ increases with increasing $y(\beta)$. In Fig. 7, we have marked the allowable ranges of $y(\beta)$ constrained by Eq. (29) for different values of $x(\alpha)$. It is evident that the bounded interval of $y(\beta)$ expands toward larger values as $x(\alpha)$ increases. Constrained by Eq. (29), when $x(\alpha)=0.3$, the permissible range of the parameter $y(\beta)$ in the Sharma-Mittal entropy is $0 \le y(\beta) \le 0.365$ (1σ) (corresponding to point A in Fig. 7(a)) and $0 \le y(\beta) \le 0.406$ (2σ) (corresponding to point B in Fig. 7(a)). When $x(\alpha)=0.4$, the corresponding range of $y(\beta)$ is $0.397 \le y(\beta) \le 0.474$ (1σ) (corresponding to points A and A' in Fig. 7(b)) and $0.366 \le y(\beta) \le 0.522$ (2σ) (corresponding to points B and B' in Fig. 7(b)). When $x(\alpha)=0.5$, the allowed values of $y(\beta)$ are $0.497 \le y(\beta) \le 0.583$ (1σ) (corresponding to points A and A' in Fig. 7(c)) and $0.462 \le y(\beta) \le 0.636$ (2σ) (corresponding to points B and B' in Fig. 7(c)).

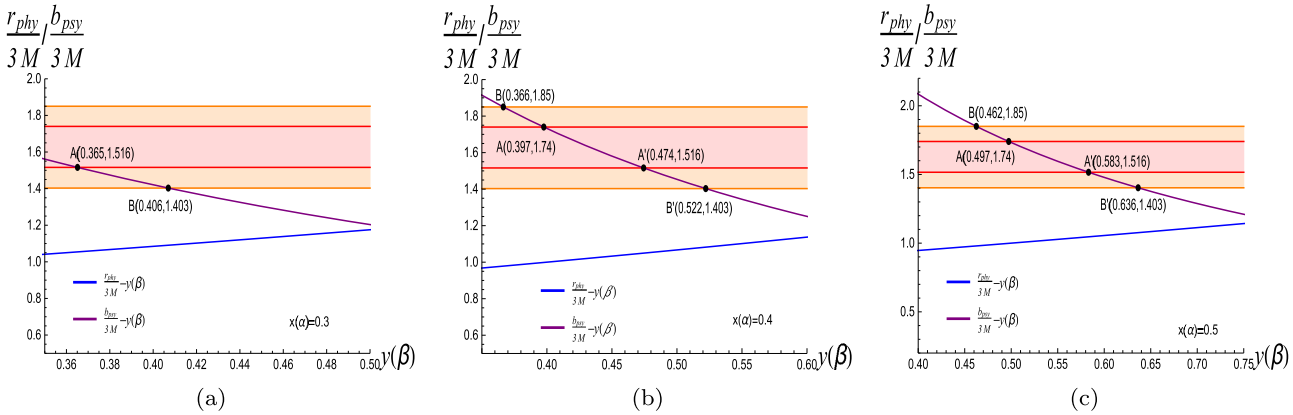


Fig. 7. (color online) The $\frac{r_{\rm phy}}{3M}-y(\beta)$ and $\frac{b_{\rm psy}}{3M}-y(\beta)$ curves for different values of $x(\alpha)$.

Figures 9 and 10 show that, for a fixed value of $y(\beta)$, the photon sphere radius $r_{{\rm ph}x}$ of the black hole associated with Sharma-Mittal entropy decreases as the correction parameter $x(\alpha)$ increases, whereas the critical impact parameter $b_{{\rm ps}x}$ grows accordingly. In addition, the maximum value of the effective potential $V_{\rm eff}$ decreases with

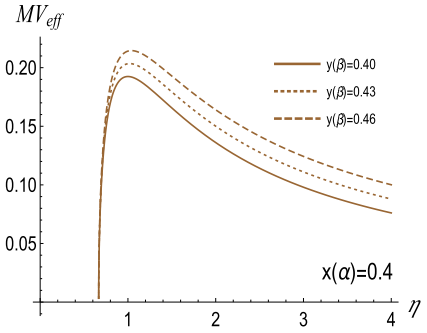


Fig. 8. (color online) The $MV_{\rm eff}-\eta$ curves for different values of $y(\beta)$ with $x(\alpha)=0.4$.

increasing $x(\alpha)$. Constrained by Eq. (29), when $y(\beta)=0.55$, the range of the parameter $x(\alpha)$ for Sharma-Mittal entropy is confined to $0.452\leq x(\alpha)\leq 0.469$ (1σ) (corresponding to points A and A' in Fig. 9(a)) and $0.424\leq x(\alpha)\leq 0.519$ (2σ) (corresponding to points B and B' in Fig. 9(a)). When $y(\beta)=0.60$, the admissible parameter range is $0.515\leq x(\alpha)\leq 0.602$ (1σ) (corresponding to points A and A' in Fig. 9(b)) and $0.468\leq x(\alpha)\leq 0.642$ (2σ) (corresponding to points B and B' in Fig. 9(b)). When $y(\beta)=0.65$, the range of the parameter $x(\alpha)$ for Sharma-Mittal entropy is confined to $0.561\leq x(\alpha)\leq 0.653$ (1σ) (corresponding to points A and A' in Fig. 9(c)) and $0.511\leq x(\alpha)\leq 0.694$ (2σ) (corresponding to points B and B' in Fig. 9(c)).

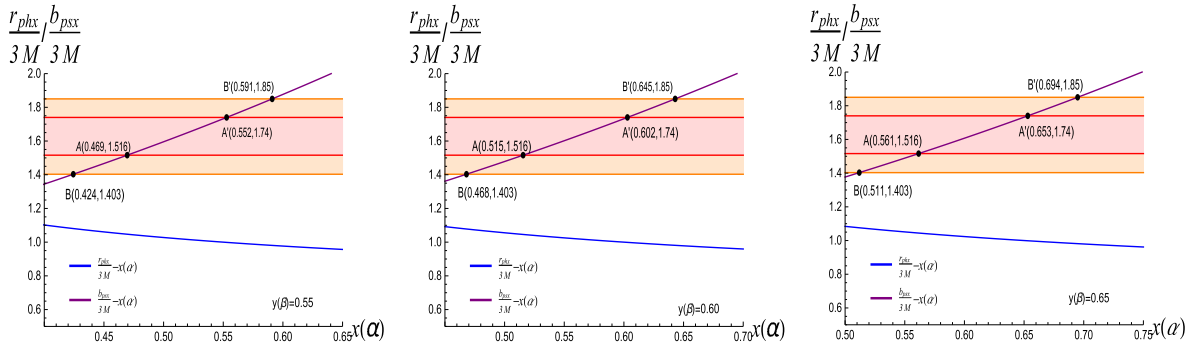


Fig. 9. (color online) The $\frac{r_{\rm phy}}{3M}-x(\alpha)$ and $\frac{b_{\rm psy}}{3M}-x(\alpha)$ curves for different values of $y(\beta)$.

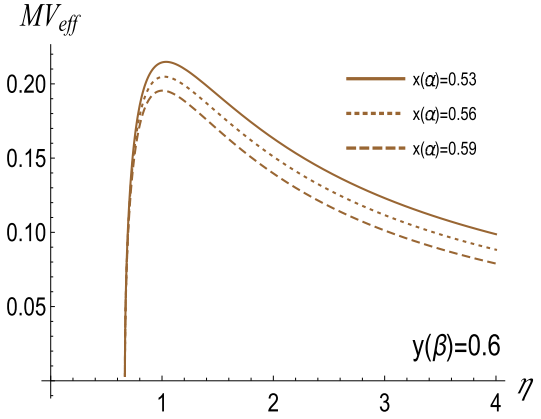


Fig. 10. (color online) The $MV_{\rm eff}-\eta$ curves for different values of $x(\alpha)$ at $y(\beta)=0.6$.

V. CONCLUSION

By investigating the photon sphere radius, critical impact parameter, and effective potential in spacetimes modified by different entropy corrections, and by comparing the numerical results with the latest Event Horizon Telescope (EHT) observations of Sagittarius A*, we constrain the admissible ranges of the characteristic parameters introduced in various entropy correction models. Accordingly, our findings provide a useful reference for further investigations of parameter constraints in modified entropy models.

In this work, we demonstrate that distinct modified entropies lead to markedly different physical results. For the Barrow entropy, an increase in the correction parameter Δ reduces the photon sphere radius $r_{\rm ph\Delta}$, increases the critical impact parameter $b_{\rm ps\Delta}$, and lowers the effective potential $V_{\rm eff}(\eta)$. For the Rényi entropy, a larger entropy correction parameter λ increases the photon sphere radius $r_{{\rm ph}\lambda}$, decreases the critical impact parameter $b_{{\rm ps}\lambda}$, and strengthens the effective potential $V_{\rm eff}(r,\lambda)$.

As illustrated in Fig. 7 and Fig. 8, for a fixed value of $x(\alpha)$, the photon sphere radius $r_{\rm phy}$ of the black hole associated with Sharma-Mittal entropy increases as the correction parameter $y(\beta)$ rises, whereas the critical impact parameter $b_{\rm psy}$ decreases accordingly. This behavior is accompanied by an increase in the maximum value of the effective potential $V_{\rm eff}(r,x)$. By contrast, as shown in Fig. 9 and Fig. 10, for a fixed value of the other Sharma-Mittal entropy parameter $y(\beta)$, an increasing correction parameter $x(\alpha)$ leads to a smaller photon sphere radius $r_{{\rm ph}x}$, a

larger critical impact parameter $b_{ps,x}$, and a lower effective potential $V_{\rm eff}(r,y)$. These results indicate that the evolutionary behaviors of the effective potential, photon sphere radius, and critical impact parameter with respect to the entropy correction parameters differ significantly among different modified entropy scenarios.

This conclusion offers valuable insights into the underlying physical nature of entropy corrections. Furthermore, the present study opens several promising avenues for future research. First, the analysis can be extended to multi-parameter and rotating black hole spacetimes to explore the optical properties of entropy-corrected black holes and broaden the scope of black hole physics research. Second, with the continuous improvement in the resolution and sensitivity of future Very Long Baseline Interferometry (VLBI) facilities, more precise constraints on the parameters of various entropy corrections can be achieved, which will further refine the relevant theoretical models. Meanwhile, our theoretical results provide timely data for comparison with increasingly accurate astrophysical observations.

References

[1] S. W. Hawking, Commun. Math. Phys. **43**, 199 (1975)
[2] J. D. Bekenstein, Phys. Rev. D **7**, 2333 (1973)
[3] R. G. Cai, S. M. Ruan, S. J. Wang *et al.*, JHEP **09**, 161 (2016), arXiv: 1606.08307[gr-qc]
[4] D. Kubizňák and R. B. Mann, JHEP **07**, 033 (2012), arXiv: 1205.0559[hep-th]
[5] R. G. Cai, L. M. Cao, L. Li *et al.*, JHEP **09**, 005 (2013), arXiv: 1306.6233[gr-qc]
[6] J. L. Zhang, R. G. Cai, H. W. Yu, Phys. Rev. D **91**, 044028 (2015), arXiv: 1502.01428[hep-th]
[7] J. P. Luminet, Astron. Astrophys. **75**, 228 (1979)
[8] F. Atamurotov, A. Abdujabbarov, and W. B. Han, Phys. Rev. D **104**, 084015 (2021)
[9] M. Biesiada, Phys. Rev. D **73**, 023006 (2006)
[10] S. Cao, M. Biesiada, R. Gavazzi *et al.*, Astrophys. J. **806**, 185 (2015), arXiv: 1509.07649[astro-ph.CO]
[11] K. Liao, Z. Li, S. Cao *et al.*, Astrophys. J. **822**, 74 (2016), arXiv: 1511.01318[astro-ph.CO]
[12] N. Tsukamoto, Phys. Rev. D **105**, 084036 (2022), arXiv: 2202.09641[gr-qc]
[13] K. Akiyama *et al.*, Astrophys. J. Lett. **875**, L6 (2019), arXiv: 1906.11243[astroph.GA]
[14] K. Akiyama *et al.*, Astrophys. J. Lett. **964**, L25 (2024), arXiv: 1906.11243[astroph.GA]
[15] K. Akiyama *et al.*, Astrophys. J. Lett. **964**, L26 (2024), arXiv: 1906.11243[astroph.GA]
[16] J. Boos and H. Hu, Phys. Rev. D **113**, 024065 (2026), arXiv: 2510.10282[gr-qc]
[17] S. Capozziello, S. De Bianchi, and E. Battista, Phys. Rev. D **109**, 104060 (2024), arXiv: 2404.17267[gr-qc]
[18] S. De Bianchi, S. Capozziello, and E. Battista, Found. Phys. **55**(3), 36 (2025), arXiv: 2504.17570[gr-qc]
[19] S. Capozziello, E. Battista, and S. De Bianchi, Phys. Rev. D **112**(4), 044009 (2025), arXiv: 2507.08431[gr-qc]
[20] A. Al-Badawi, F. Ahmed, and İzzet. Sakallı, arXiv: 2604.01255[gr-qc]
[21] J. M. Ladino, C. E. Romero-Figueroa, and H. Quevedo, Eur. Phys. J. C **86**(7), 748 (2026), arXiv: 2604.01521[gr-qc]
[22] C. Y. Yang, X. X. Zeng, arXiv: 2604.00117[gr-qc]
[23] E. Battista, S. Capozziello, and C. Y. Yang, Phys. Rev. D **113**(10), 104039 (2026), arXiv: 2601.10806[gr-qc]
[24] C. K. Qiao, Eur. Phys. J. C **85**, 191 (2025), arXiv: 2407.14035[gr-qc]
[25] X. X. Zeng, H. Ye, M. I. Aslam *et al.*, arXiv: 2603.07185[gr-qc]
[26] X. X. Zeng, Y. Hong, and K. Wang, arXiv: 2602.21836[gr-qc]
[27] X. X. Zeng, C. Y. Yang, M. I. Aslam *et al.*, Eur. Phys. J. C **86**(4), 383 (2026), arXiv: 2511.00586[gr-qc]
[28] X. X. Zeng, C. Y. Yang, and H. Yu, Eur. Phys. J. C **85**, 1242 (2025), arXiv: 2508.03020[gr-qc]
[29] X. X. Zeng, L. F. Li, P. Li *et al.*, Sci. China. Phys. Mech. **68**, 220412 (2025), arXiv: 2411.12528[gr-qc]
[30] B. F. Wu, E. W. Liang, and X. Zhang, Eur. Phys. J. C **85**, 632 (2025), arXiv: 2501.00361[gr-qc]
[31] X. X. Zeng, H. Q. Zhang, and H. Zhang, Eur. Phys. J. C **80**, 872 (2020), arXiv: 2004.12074[gr-qc]
[32] S. W. Wei, C. H. Wang, Y. P. Zhang *et al.*, arXiv: 2601.15612[gr-qc]
[33] J. W. Li, Z. L. Wang, and T. T. Sui, Eur. Phys. J. C **86**, 335 (2026), arXiv: 2603.09159[gr-qc]
[34] T. Y. Zhang, Z. Y. Qin, Q. Feng *et al.*, arXiv: 2603.09105[astro-ph.HE]
[35] R. Berens, P. Galison, T. Gravely *et al.*, arXiv: 2603.08790[gr-qc]
[36] S. Hod, Phys. Rev. D **113**(2), 024064 (2026), arXiv: 2603.03421[gr-qc]
[37] S. W. Wei and Y. X. Liu, Phys. Dark Univ. **43**, 101409 (2024), arXiv: 2308.11883[gr-qc]
[38] S. B. Chen, J. L. Jing, W. L. Qian *et al.*, Sci. China Phys. Mech. Astron. **66**, 260401 (2023), arXiv: 2301.00113[astro-ph.HE]
[39] Y. Y. Wang, M. D. Zhao, X. Y. Wang *et al.*, Eur. Phys. J. C **86**(7), 803 (2026), arXiv: 2511.06219[gr-qc]
[40] C. Bambi, K. Freese, S. Vagnozzi *et al.*, Phys. Rev. D **100**(4), 044057 (2019), arXiv: 1904.12983[gr-qc]
[41] M. Khodadi, S. Vagnozzi, and J. T. Firouzjaee, Sci. Rep. **14**(1), 26932 (2024), arXiv: 2408.03241[gr-qc]
[42] P. K. Yerra and C. Bhamidipat, Class. Quant. Grav. **43**(7), 075005 (2026), arXiv: 2509.04261[gr-qc]
[43] J. L. Chen, S. P. Wu, and S. W. Wei, Phys. Lett. B **880**(7), 140712 (2026), arXiv: 2510.23047[gr-qc]
[44] W. T. Liu, Y. Liu, D. Wu *et al.*, arXiv: 2511.06017[gr-qc]
[45] A. Errehymy, Phys. Lett. B (870), 139945 (2025)
[46] K. J. He, H. Ye, X. X. Zeng *et al.*, Chin. Phys. **49**(12), 125103 (2025), arXiv: 2502.08388[gr-qc]
[47] S. Roy, S. Chatterjee, and R. Koley, Eur. Phys. J. C **84**(1), 47 (2024), arXiv: 2309.02709[gr-qc]
[48] M. I. Aslama and R. Saleemb, Eur. Phys. J. C **84**, 37 (2024)
[49] H. Lekbich, N. Parbin, D. J. Gogoi *et al.*, Eur. Phys. J. C **84**, 350 (2024)
[50] A. Sadeghi and F. Shoja, arXiv: 2602.10269[gr-qc]

[51] Z. Y. Li, S. Q. Liu, and J. H. Huang, Chin. Phys. C **50**(7), 075105 (2026), arXiv: 2602.14458[astro-ph.HE]

[52] Y. Z. Du, H. F. Li, F. Liu *et al*., JHEP **01**, 137 (2023), arXiv: 2204.01007[hep-th]

[53] Y. Z. Du, H. F. Li, Y. B. Ma *et al*., Eur. Phys. J. C **85**, 78 (2025)

[54] J. Sharipov, J. Khasanov, P. Sheoran *et al*., arXiv: 2602.09168[gr-qc]

[55] F. Ahmed, A. Al-Badawi, and M. Fathi, Eur. Phys. J. C **86**(6), 658 (2026), arXiv: 2601.10469[gr-qc]

[56] S. N. Gashti, M. A. S. Afshar, M. R. Alipour *et al*., Eur. Phys. J. C **85**(10), 1144 (2025), arXiv: 2504.11939[hep-th]

[57] C. Promsiri, E. Hirunsirisawat, and W. Liewrian, Phys. Rev. D **102**(10), 064014 (2020)

[58] U. Zafar, A. Jawad, K. Bamba *et al*., Gen. Rel. Grav. **58**(3), 30 (2026), arXiv: 2603.00916[gr-qc]

[59] K. J. He, G. P. Li, L. F. Li *et al*., arXiv: 2603.27606[gr-qc]

[60] H. E. Gong, J. L. Qin, Y. S. Wang *et al*., Chin. Phys. C **50**, 085101 (2026), arXiv: 2508.20419[gr-qc]

[61] M. F. Fauzi, H. S. Ramadhan, and A. Sulaksonoi, Phys. Lett. B **875**, 140367 (2026), arXiv: 2512.17304[gr-qc]

[62] R. C. de Paiva, K. S. Alves, R. T. Cavalcanti *et al*., Annals Phys. **492**, 170540 (2026), arXiv: 2512.14920[gr-qc]

[63] F. Ahmed, S. Murodov, B. Rahmatov *et al*., arXiv: 2602.22264[gr-qc]

[64] C. F. S. Pereira, M. V. de S. Silva, A. R. Soares *et al*., Phys. Lett. B **879**, 140699 (2026), arXiv: 2602.22905[gr-qc]

[65] M. A. Resco, Phys. Dark Univ. **51**, 102189 (2026), arXiv: 2510.00702[gr-qc]

[66] H. L. Zhen, J. H. Shi, H. F. Li *et al*., Phys. Lett. B **877**, 140488 (2026), arXiv: 2603.03660[gr-qc]

[67] J. Peng, M. Guo, and X. H. Feng, Chin. Phys. C **45**, 085103 (2021), arXiv: 2008.00657[gr-qc]

[68] H. L and H. D. Lyu, Phys. Rev. D **101**, 044059 (2020)

[69] S. Guo, Y. X. Huang, Y. H. Cui *et al*., Eur. Phys. J. C **83**, 1059 (2023)

[70] X. X. Zeng, K. J. He, G. P. Li *et al*., Eur. Phys. J. C **82**, 764 (2022)

[71] S. Nojiri, S. D. Odintsov, and V. Faraoni, Phys. Rev. D **104**(8), 084030 (2021), arXiv: 2109.05315[gr-qc]

[72] S. Nojiri, S. D. Odintsov, and V. Faraoni, Int. J. Geom. Meth. Mod. Phys. **19**(13), 2250210 (2022), arXiv: 2207.07905[gr-qc]

[73] E. Elizalde, S. Nojiri, and S. D. Odintsov, Universe **11**(2), 60 (2025), arXiv: 2502.05801[gr-qc]

[74] H. X. Lu, S. D. Gennaro, and Y. C. Ong, Annals Phys. **474**, 169914 (2025), arXiv: 2407.00484[gr-qc]

[75] A. Anand, S. Devdutt, K. Jusufi *et al*., Eur. Phys. J. C **86**(5), 534 (2026), arXiv: 2511.04613[gr-qc]

[76] A. Anand, K. Jusuff, S. Basilakos *et al*., Eur. Phys. J. C **86**(2), 126 (2026), arXiv: 2512.13769[gr-qc]

[77] A. Anand and S. N. Gashti, Phys. Dark Univ. **49**, 102018 (2025), arXiv: 2507.21663[gr-qc]

[78] A. Anand and S. N. Gashti, Phys. Dark Univ. **49**, 102015 (2025), arXiv: 2411.02875[gr-qc]

[79] S. N. Gashti and B. Pourhassan, Eur. Phys. J. C **85**, 435 (2025), arXiv: 2412.12132[hep-th]

[80] J. D. Barrow, Phys. Lett. B **808**, 135643 (2020), arXiv: 2004.09444[gr-qc]

[81] A. Rényi, *Proceedings of the Fourth Berkeley Symposium on Mathematical Statistics and Probability 1: Contributions to the Theory of Statistics*, 547-561, (1961)

[82] A. Majhi, Phys. Lett. B **775**, 32 (2017), arXiv: 1703.09355[gr-qc]

[83] A. S. Jahromi, S. A. Moosavi, H. Moradpour *et al*., Phys. Lett. B **780**, 21 (2018), arXiv: 1802.07722[gr-qc]

[84] M. A. S. Afshar, M. R. Alipour, S. N. Gashti *et al*., Eur. Phys. J. C **85**, 457 (2025), arXiv: 2501.00955[gr-qc]

[85] S. N. Gashti, JHAP **4**(4), 59 (2024)

[86] A. Errehymy, Y. Khedif, M. Daoud *et al*., Phys. Lett. B **870**, 139915 (2025), arXiv: 2509.17630[gr-qc]

[87] C. K. Qiao and M. Li, Phys. Rev. D **106**, L021501 (2022), arXiv: 2204.07297[gr-qc]

[88] C. K. Qiao, Phys. Rev. D **106**(8), 084060 (2022), arXiv: 2208.01771[gr-qc]

[89] R. Carballo-Rubio, F. D. Filippo, S. Mukohyama *et al*., JHEP **02**, 129 (2026), arXiv: 2509.10667[gr-qc]

[90] S. Vagnozzi *et al*., Class. Quant. Grav. **40**, 165007 (2023), arXiv: 2205.07787[gr-qc]

[91] R. C. Pantig, Ali Övgün, and Durmuş Demir, Eur. Phys. J. C **83**, 250 (2023), arXiv: 2208.02969[gr-qc]

[92] X. X. Zeng, C. Y. Yang, M. I. Aslam *et al*., JCAP **28**, 066 (2025), arXiv: 2505.07063[gr-qc]